



## ISTITUTO NAZIONALE DI RICERCA METROLOGICA Repository Istituzionale

Spectral Emission Dependence of Tin-Vacancy Centers in Diamond from Thermal Processing and Chemical Functionalization

*Original*

Spectral Emission Dependence of Tin-Vacancy Centers in Diamond from Thermal Processing and Chemical Functionalization / Corte, Emilio; Sachero, Selene; Ditalia Tchernij, Sviatoslav; Lühmann, Tobias; Pezzagna, Sébastien; Traina, Paolo; Degiovanni, Ivo Pietro; Moreva, Ekaterina; Olivero, Paolo; Meijer, Jan; Genovese, Marco; Forneris, Jacopo. - In: ADVANCED PHOTONICS RESEARCH. - ISSN 2699-9293. - 3:1(2021), p. 2100148. [10.1002/adpr.202100148]

*Availability:*

This version is available at: 11696/72916 since: 2022-02-11T14:00:26Z

*Publisher:*

Wiley-VCH

*Published*

DOI:10.1002/adpr.202100148

*Terms of use:*

This article is made available under terms and conditions as specified in the corresponding bibliographic description in the repository

*Publisher copyright*

(Article begins on next page)

# Spectral Emission Dependence of Tin-Vacancy Centers in Diamond from Thermal Processing and Chemical Functionalization

Emilio Corte, Selene Sachero, Sviatoslav Ditalia Tchernij,\* Tobias Lühmann, Sébastien Pezzagna, Paolo Traina, Ivo Pietro Degiovanni, Ekaterina Moreva, Paolo Olivero, Jan Meijer, Marco Genovese, and Jacopo Forneris\*

A systematic photoluminescence (PL) investigation of the spectral emission properties of individual optical defects fabricated in diamond upon ion implantation and annealing is reported. Three spectral lines at 620, 631, and 647 nm are identified and attributed to the SnV center due to their occurrence in the PL spectra of the very same single-photon emitting defects. It is shown that the relative occurrence of the three spectral features can be modified by oxidizing the sample surface following thermal annealing. The relevant emission properties of each class of individual emitters, including the excited state emission lifetime and the emission intensity saturation parameters are reported.

## 1. Introduction

Diamond-based color centers are appealing candidates as solid-state single-photon sources for applications in emerging fields of quantum technologies, such as quantum computing, quantum information, and quantum sensing.<sup>[1–5]</sup> A class of group-IV-

related quantum emitters, fabricated upon Sn ion implantation, thermal annealing, and surface oxidation was recently discovered.<sup>[6,7]</sup> These color centers exhibit intriguing opto-physical properties, such as high emission rate, narrow spectral width, and emission concentrated in the zero-phonon line (ZPL), thus sparking the interest of the scientific community toward practical applications in the field of quantum technologies,<sup>[4]</sup> including quantum sensing,<sup>[8]</sup> nanophotonics,<sup>[9]</sup> and spintronics.<sup>[10,11]</sup>

The characteristic spectral feature of the optical activity of the SnV center consists of

a strong room-temperature ZPL emission at 620 nm, which is widely attributed to the negative charge state of the defect (SnV) based on the convincing support of independent theoretical works based on *ab initio* simulations.<sup>[6,11,12]</sup> In addition, multiple works have independently observed additional emission lines at 593 nm,<sup>[6,7,13,14]</sup> 631 nm,<sup>[7,14,15]</sup> 647 nm,<sup>[6–8,13–15]</sup> and 663 nm.<sup>[12,14,15]</sup>

While the 663-nm line has been convincingly interpreted as a radiation-induced defect,<sup>[12,15]</sup> the attribution of the remaining photoluminescence (PL) peaks is still uncertain and requires further disambiguation. DFT simulations have highlighted the possibility to observe the SnV center in different charge states,<sup>[11,16]</sup> however a conclusive model of the experimental findings according to this interpretation has not been achieved yet. Recent reports on this subject suggest that the aforementioned emission lines are originating from different Sn-containing lattice complexes.<sup>[6,8,9]</sup> In these works the defects are created by ion irradiation, and different experimental conditions (ion implantation energy, annealing temperature and duration, and chemical termination of the latter) are explored. In particular, it is worth noting that the ion irradiation parameters result in different depth distributions of the defects, as well as their distance from the surface. Remarkably, high-pressure/high-temperature annealing processing performed without specific additional surface treatments resulted in the observation of the sole 620 nm emission line.<sup>[6]</sup> Moreover, the excitability of the 647 nm line under 633 nm laser excitation provided a strong experimental indication that such spectral feature cannot be attributed to the negative charge state of the SnV defect (620 nm ZPL).<sup>[15]</sup>


Finally, the electrical control of the Fermi level of an O-terminated p-i-p diamond junction has shown that all the

E. Corte, S. Ditalia Tchernij, P. Olivero, J. Forneris  
Dipartimento di Fisica, Università degli Studi di Torino, Istituto Nazionale di Fisica Nucleare (INFN), Sez. Torino  
Istituto Nazionale di Ricerca Metrologica (INRiM)  
via P. Giuria 1, 10125 Torino, Italy  
E-mail: sviatoslav.ditalia@unito.it; jacopo.forneris@unito.it

S. Sachero  
Dipartimento di Fisica  
Università degli Studi di Torino  
via P. Giuria 1, 10125 Torino, Italy

T. Lühmann, S. Pezzagna, J. Meijer  
Applied Quantum Systems, Felix-Bloch Institute for Solid-State Physics  
Universität Leipzig  
Linnéstraße 5, 04103 Leipzig, Germany

P. Traina, I. P. Degiovanni, E. Moreva, M. Genovese  
Division of Quantum Metrology and Nanotechnologies  
Istituto Nazionale di Ricerca Metrologica (INRiM)  
Strada delle Cacce 91, 10135 Torino, Italy

 The ORCID identification number(s) for the author(s) of this article can be found under <https://doi.org/10.1002/adpr.202100148>.

© 2021 The Authors. Advanced Photonics Research published by Wiley-VCH GmbH. This is an open access article under the terms of the Creative Commons Attribution License, which permits use, distribution and reproduction in any medium, provided the original work is properly cited.

DOI: 10.1002/adpr.202100148

620, 631, and 647 nm could be identified at the single-photon emitter level, but those spectral features were observed only from separate defects.<sup>[14]</sup>

In this work, we compare the room-temperature properties of single emitters in a Sn-ion-implanted diamond sample following different post-implantation processing treatments. Particularly, we report the concurrent observation of the 620, 631, and 647 nm from the same individual emitter after a thermal annealing process that was not followed by a chemical functionalization of the diamond surface. We also discuss the variation in the relative population of the emission lines in a discrete set of single centers upon the subsequent O-termination of the sample surface by means of plasma treatments. Finally, we report a characterization of the aforementioned lines at the single-photon emitter level. These results offer promising perspectives towards the chemical control of the emission properties of Sn-related defects in diamond.

## 2. Results

### 2.1. Sn-Related Emitters Formed upon Thermal Annealing

We report in this section the characterization of the emitters upon the sole thermal annealing, that is, without any further surface functionalization. **Figure 1a** shows a typical PL map (13 × 13 μm<sup>2</sup> area, 60 μW excitation power) acquired from the region under investigation,<sup>[29]</sup> showing a density of ≤1 μm<sup>-2</sup> bright luminescent spots, whose emission was investigated individually. The discussion in the following text is focused on those sole spots (≈30), where HBT interferometry confirmed a second-order auto-correlation function  $g^{(2)}(t=0) < 0.25$  after background correction.<sup>[7]</sup> Consistently with what observed in the reports discussed in Section 1, three main groups of spectral lines were observed, corresponding to the emission at 620 nm (S1), 631 nm (S2), and 647 nm (S3). Selected spectra are reported

in **Figure 1b**, highlighting that the S1–S3 emission lines could be observed both separately (i–iii) as the sole spectral feature of the considered center, as well as concurrently in the emission spectra of the same individual single-photon emitter. Particularly, **Figure 1b-iv, v, and vi** show the spectra of single-photon emitters exhibiting both the “S1 and S2”, “S1 and S3”, “S2 and S3” spectral features at the same time, respectively. **Figure 2a** (grey dots refer to the as-annealed sample) shows the spectral position of the emission lines acquired during the PL characterization, evidencing a non-negligible (i.e., ≈25%) occurrence of multiple emission lines among the S1–S3 set from the same point defect. The reported peaks were identified using a spectral analysis routine relying on first derivative analysis. A threshold for noise discrimination was set to select only those peaks having a prominence with respect to the baseline higher than 10% the prominence of the most intense peak.

To provide further insight into the aforementioned discussion, we report in **Figure 3a** the PL spectrum of an individual emitter concurrently exhibiting the S1 and S3 emission peaks. **Figure 3b** shows the  $g^{(2)}(t)$  acquired from the center under 0.27 mW laser excitation. The antibunching at  $t=0$  (background-corrected  $g^{(2)}(0)=0.11 \pm 0.11$ , considering a signal-to-background ratio<sup>[6,7]</sup> of  $\rho = 0.49 \pm 0.05$ ) indicates that the emission originates from an individual lattice defect.<sup>[30]</sup>

Conversely in **Figure 3c** we report the PL spectrum of a diffraction-limited spot where both the S2 and S3 line could be observed. The antibunching behavior was denoted by a value of  $g^{(2)}(0) = 0.04 \pm 0.09$  upon background subtraction ( $\rho = 0.55 \pm 0.07$ ), confirming that also in this case the emission originates from the very same emitter.

Based on this analysis, the concurrent observation of the pairs of spectral features (S1 and S3; S2 and S3) individual emitters suggests that all the three emission lines are to be referred to the same localized lattice defect.

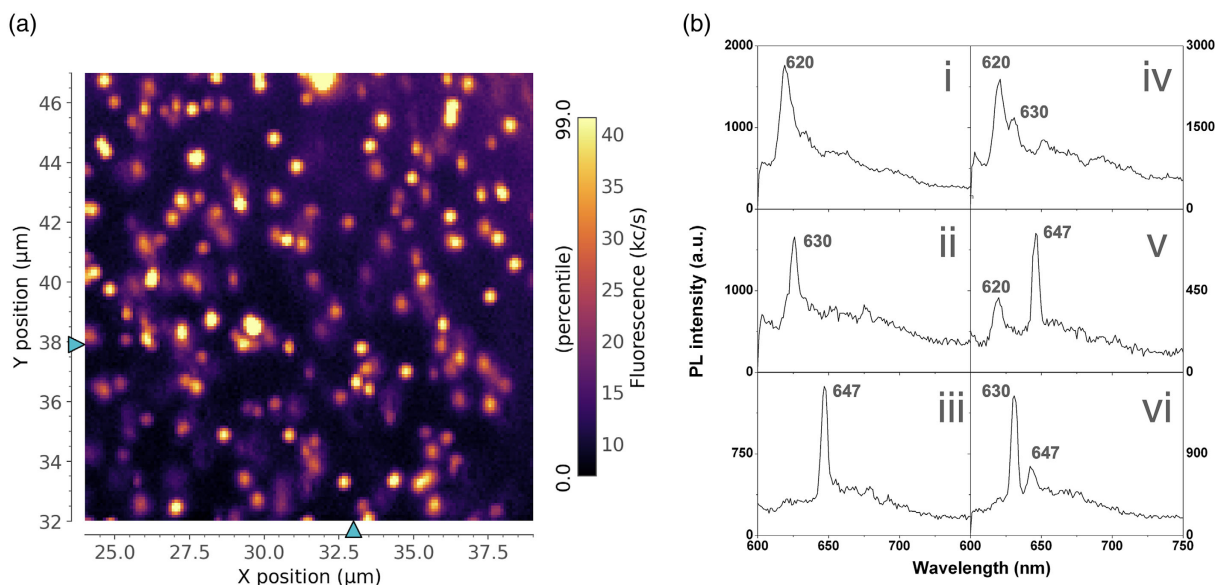


**Figure 1.** a) Typical confocal PL map acquired under 520 nm laser excitation (60 μW power on the sample) from the Sn-implanted region of interest of the sample. b) PL spectra from individual emitters exhibiting emission lines at: i) 620 nm, ii) 631 nm, iii) 647 nm, iv) 620 and 631 nm; v) 620 and 647 nm, and vi) 631 and 647 nm.

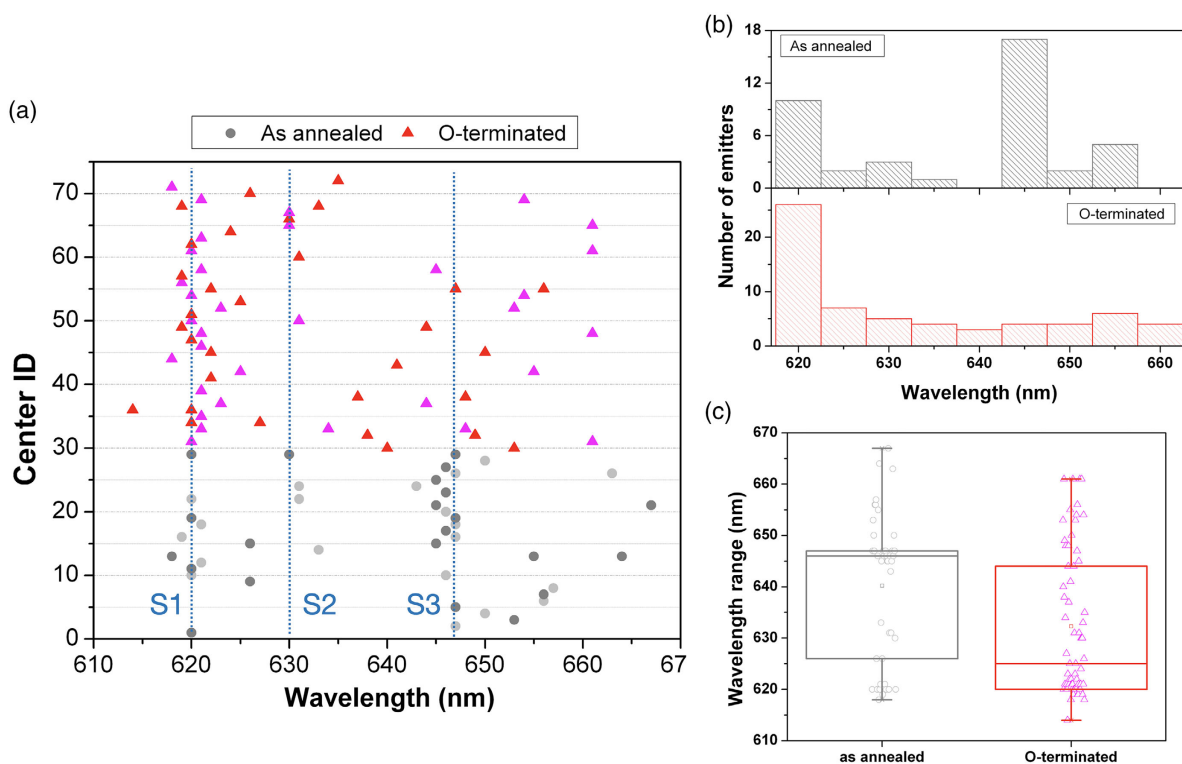


**Figure 2.** a) Summary of the spectral position of the main emission lines acquired from a set of individual diffraction-limited emitting spots in the Sn-implanted region of the sample. Both light and dark grey dots refer to the as-annealed sample; the alternate color code is chosen to highlight the occurrence of multiple emission lines from individual emitting spots. Red and magenta dots refer to emitters observed in the sample upon oxygen plasma treatment. b) Histograms of the occurrence of emission lines relative to the dataset shown in a). Grey and red bars refer to the as-annealed and oxygen-terminated sample, respectively. c) Box chart of the emission lines distribution extracted from the datasets in a).

## 2.2. Sn-Related Emitters Characterization upon Surface O-Termination

We report the PL characterization of the emitters in the region of interest of the sample following the  $O_2$  plasma treatment described in Section 2. The O-termination of the sample required to unmount the sample from the confocal microscope. After this process the same region of the sample was investigated, but a study of the very same emitters studied in the previous experimental campaigns could not be performed. The interpretation of the data therefore rely on the assumption that the occurrence of the spectral lines is homogeneous in the whole region of interest, provided that the same density of centers per surface unit was observed. Additional characterizations performed after an  $O_2$  plasma treatment performed at a higher microwave power (40 W) provided results statistically comparable with those reported here. Figure 2a shows the spectral position of the PL lines observed over a set of  $\approx 40$  emitters upon O-termination of the surface (red scatter data). The data indicate an apparent increase in the relative population of the S1 emission line, concurrently with a significant decrease in that of the S2 peak. This observation is further corroborated by the histogram shown in Figure 2b showing the occurrence of the spectral lines as a function of the emission wavelength observed after thermal annealing (gray bars) and after plasma treatment (red).

The “as annealed” sample reveals a prevalence of the S3 line ( $\approx 40\%$  of the total amount of the observed lines) with respect to the S1 (25%). Such distribution is completely reversed in the O-terminated configuration, in which S1 becomes the most observed spectral feature ( $\approx 40\%$ ), the S3 emission being associated to a mere 6% of the counts. Such observation is more evidenced by the box chart shown in Figure 2c. Here, the median of the “as annealed” sample ZPL distribution (gray) coincides with the S3 emission line, while the range of spectra features compatible with the S1 line define the Q2–Q1 interquartile for the “O-terminated” data (red).

These data, together with the concurrent observation of both S1 and S3 lines from the very same individual defect, might be suggestive of their attribution to different charge states of the same defect. Particularly, the S1 line has been unambiguously attributed to the negative charge state of the tin-vacancy center  $SnV^{[6,11]}$ . The prevalence of this line upon O-termination of the diamond surface is also in line with what already reported for the nitrogen-vacancy center (NV), whose negative charge state is stabilized upon chemical functionalization by elements with positive electron affinity.<sup>[31]</sup> However, a direct comparison with the charge state population of NV centers could not be performed due to the scarce amount of these defects in the sample under investigation. Furthermore, previous attempts to dynamically switch the S1 and S3 emission upon the electrical tuning of

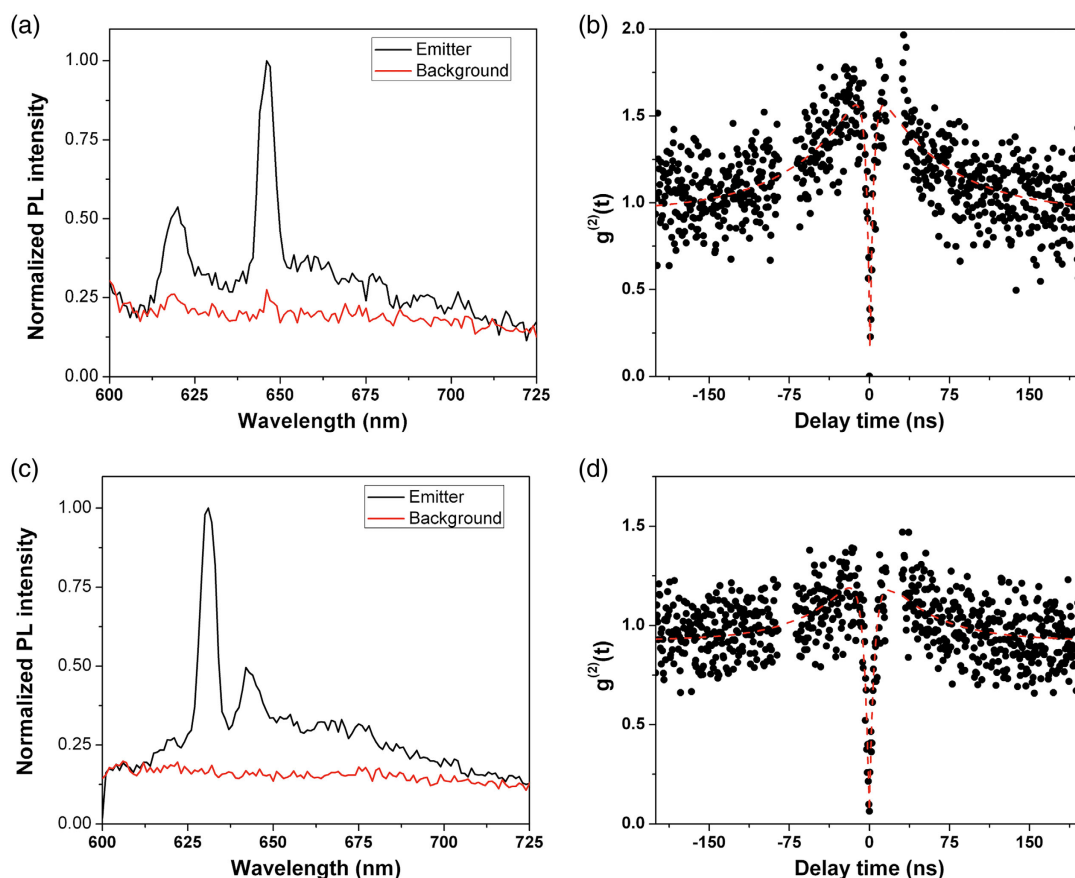


**Figure 3.** a) Emission spectrum from a diffraction-limited emission spot (black line) showing the S1 and S3 lines. The red line indicates the background emission spectrum acquired from a low-intensity emission spot placed in closed proximity of the probed emitter. The black line does not take into account background subtraction. b) Corresponding background-corrected second-order autocorrelation function  $g^{(2)}(t)$ . c) Emission spectrum from a diffraction-limited emission spot (black line) showing the S2 and S3 lines, and d) corresponding background-corrected  $g^{(2)}(t)$  function. Both  $g^{(2)}(t)$  functions were measured under 520 nm laser excitation (0.27 mW power). The missing datapoint around  $-75$  and  $+20$  ns delay time correspond to the backflash peaks of the HBT interferometer,<sup>[40]</sup> which were removed for ease of view.

the diamond Fermi level down to 4.6 eV below the conduction band<sup>[14]</sup> suggest that S3 line might not be identified with the  $\text{SnV}^0$  charge state. Therefore, the attribution of the S3 line to the interaction of the SnV center with surrounding defects resulting from an incomplete annealing of the crystal lattice upon ion implantation, could not be disregarded under the parameters adopted for the sample processing.<sup>[6]</sup>

Photon count rate blinking could not be adopted as a criterion to discriminate among these two possible attributions. On the one hand, indeed, blinking is often linked with both charge state conversion and non-resonant energy transfer to surrounding defects.<sup>[32,33]</sup> On the other hand, count rate blinking (few to tens of seconds time scales) was indeed observed even from several defects exhibiting one spectral line only upon sufficiently high excitation power ( $>200 \mu\text{W}$ ). Conversely, several diffraction-limited spots exhibiting multiple spectral components showed stable count rates over tens of seconds of observation. Finally, the spectral measurements were acquired using a scanning monochromator, so that the simultaneous monitoring over time

of the three main emission lines was not possible due to the given constraints of the experimental setup.

The histogram shown in Figure 2b does not reveal further significant spectral components, neither in the as-annealed sample, nor following the subsequent surface oxidation. Both the S2 and the 660 nm lines are observed, although their occurrence is significantly smaller than that of the S1 and S3 spectral features (S2: 7% as-annealed, 8% O-terminated; 660 nm: 12% as annealed, 9% O-terminated).

It is also worth mentioning that 7% of the identified emission lines in the as-annealed sample does not correspond to the S1 or S3 lines, but occur in the spectral range comprised between 620 and 635 nm. Such fraction increases to 35% if the lines in the 625–655 nm range are considered for the O-terminated sample. This observation might not be incompatible with the hypothesis that the SnV center is not fully formed under the adopted low-pressure high-temperature annealing process,<sup>[5,6]</sup> or with the interpretation of the ZPL spectral diffusion as a consequence of the radiation-induced local strain interacting with the defects.



### 2.3. Characterization of Emitters with S1, S2, and S3 Spectral Features

Individual Sn-related centers evidencing a single emission line were studied systematically to assess the respective emission properties in the “as annealed” sample. The properties observed at the single-photon emitter level did not reveal significant differences upon O-termination of the surface, in addition to the occurrence of each spectral line.

We report the results acquired from individual emitters exhibiting only one spectral feature, that is, the S1, S2, and S3 line only, respectively.

Each of these defects was characterized by acquiring the second-order auto-correlation function curve at different optical excitation powers. Each of these curves underwent a fitting procedure according to a three-level system based on the following equation<sup>[7,34]</sup>:

$$g^{(2)}(t) = 1 - a_1 \exp(-|t|\lambda_1) + a_2 \exp(-|t|\lambda_2) \quad (1)$$

where the term proportional to  $a_1$  describes the nonclassical antibunching signature of quantum emitters. The  $\lambda_1$  parameter was fitted against the excitation power  $P$  according to a linear model to infer the lifetime of the excited state as  $\tau = [\lambda_1(P=0)]^{-1}$ .

We also studied the emission intensity  $I$  of the defect as a function of the optical excitation power, to establish a preliminary comparison of the relevant emission properties of the three

spectral components on the basis of those, already discussed in the literature, of the S1 line. The emission intensity was modelled after the expression<sup>[7,35]</sup>

$$I(P) = I_{\text{sat}} \cdot P / (P + P_{\text{sat}}) \quad (2)$$

where  $I_{\text{sat}}$  and  $P_{\text{sat}}$  are the saturation intensity and the saturation excitation power, respectively.

#### 2.3.1. S1—620 nm Emission Line

The characterization of the defect emitting at 620 nm ZPL (from whom the PL spectrum “i” reported in Figure 1b was acquired) is shown in **Figure 4**.  $g^{(2)}(t)$  curves acquired in the 0.27–0.43 mW excitation power range (Figure 4a) are reported as an example. The linear fitting of the  $\lambda_1$  parameter (Figure 4b) resulted in an estimation of the radiative emission lifetime of  $\tau = (6.0 \pm 0.8)$  ns, a value fully compatible with what reported in previous works and attributed to the ZPL of the SnV<sup>+</sup> center.<sup>[6,7,36]</sup> Similarly, the center’s deshelling lifetime was estimated by a linear regression of the dependence of  $\lambda_2$  on the laser excitation power (Figure 4c) as  $\tau_2 = \lambda_2(0)^{-1} = (68 \pm 9)$  ns. The analysis upon background subtraction of the emission intensity saturation curve (Figure 4d) resulted in an excitation saturation power  $P_{\text{sat}} = (0.32 \pm 0.07)$  mW. This value is compatible with what reported in ref. [7], considering that the  $(1.11 \pm 0.01)$  mW value reported there quantified the laser power

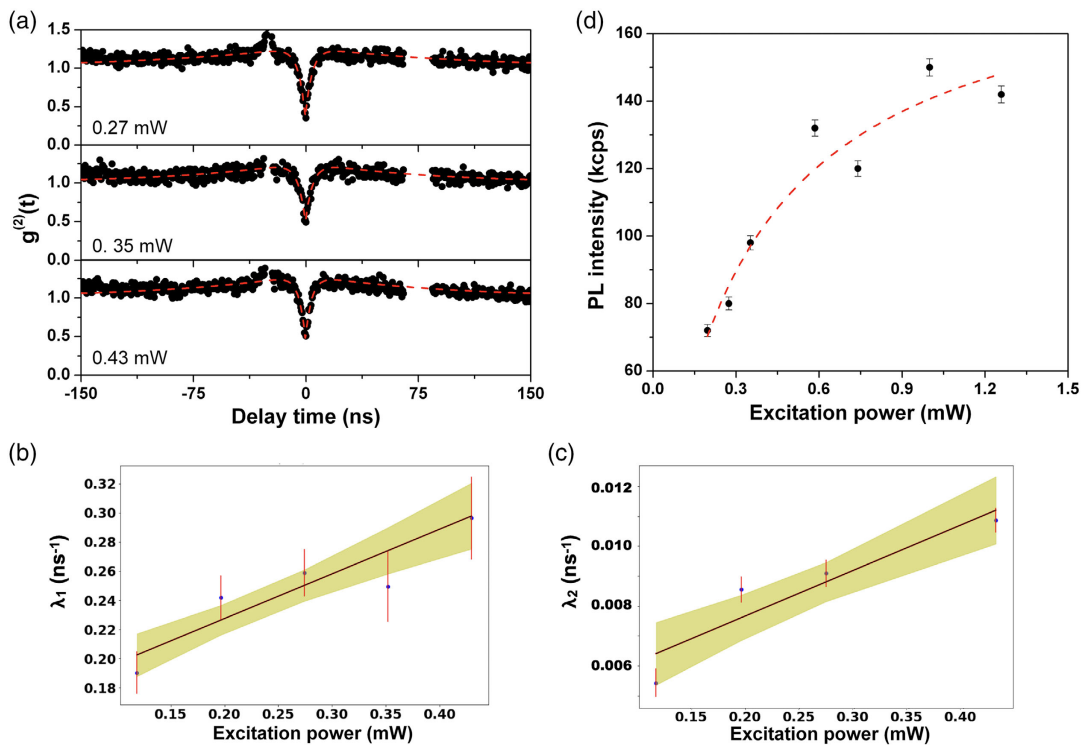


**Figure 4.** Characterization of the single-photon emission properties of an individual Sn-related defect emitting at the S1 line (620 nm), corresponding to the PL spectrum iii in Figure 1b. a) Second-order auto-correlation functions ( $g^{(2)}(t)$  curves shown without background-correction) acquired under 0.27, 0.35, and 0.43 mW laser excitation power. b) Linear fit of the decay constant  $\lambda_1$  extracted from the function fit of the  $g^{(2)}(t)$  curves as a function of the excitation power. Red lines represent the fitting curves. c) Linear fit of the deshelling state lifetime parameter as a function of the laser excitation power. d) Background-subtracted emission rate as a function of the laser excitation power. The red dashed line represents the fitting curve.

incident on the microscope objective. A decrease of  $\approx 60\%$  in the power transmitted to the sample was observed in the confocal microscope adopted in this work. The saturation emission intensity  $I_{\text{sat}} = (186 \pm 15)$  kcps was an order of magnitude lower than what reported in the previous characterization of this emission line.<sup>[7]</sup> This discrepancy is ascribed to the fiber-coupling of the source in the confocal microscope adopted for the present study, to be compared with the adoption of a higher-efficiency air-coupling of single-photon detectors in the referenced work. While a direct comparison between the two experiments cannot be performed without a metrological calibration of the two experimental apparatuses, the value obtained in this work could be used as a reference to assess the relative intensity of the S2 and S3 emission lines with respect to the bright<sup>[6,7]</sup> emission of the 620 nm peak.

### 2.3.2. S2—631 nm Emission Line

A defect emitting at 631 nm (PL spectrum “ii” in Figure 1b) was characterized against the same emission properties (Figure 5). The acquisition of  $g^{(2)}(t)$  curves in the 0.27–0.59 mW excitation power range (Figure 5a) enabled a preliminary estimation of the center lifetime as  $\tau_1 = \lambda_1(0)^{-1} = (4.8 \pm 1.7)$  ns (Figure 5b). Despite the value being compatible with that of the S1 line, the saturation emission intensity (Figure 5c) displayed a significantly higher value of  $I_{\text{sat}} = (300 \pm 40)$  kcps achieved at a compatible excitation saturation power  $P_{\text{sat}} = (0.42 \pm 0.08)$  mW.

### 2.3.3. S3—647 nm Emission Line

The  $g^{(2)}(t)$  curves relative to the 647 nm emission of a defect associated with the PL spectrum “iii” in Figure 1b are shown in Figure 6a for the 0.27–0.59 mW excitation power range. The measurements enabled to quantify the center’s excited state lifetime as  $\tau_1 = (7.4 \pm 1.0)$  ns (Figure 6b).

It is also worth noting that the  $\lambda_2$  parameter (Figure 6c) exhibits a decreasing trend at increasing excitation power, a behavior which is not usually observed in diamond quantum emitters.<sup>[37,38]</sup> The deshelling lifetime was estimated from the intercept parameter of the linear regression in Figure 6b as  $\tau_2 = \lambda_1(0)^{-1} = (68 \pm 9)$  ns.

The unusual behavior observed for the emitter can be tentatively attributed to the power-dependent depletion of the shelving state in favor of a fourth, excited state.<sup>[37]</sup> This interpretation would be in line with the attribution of the S3 emission to the interaction of the SnV center with a surrounding radiation-induced defect. However, an unambiguous attribution of this phenomenon, such as the identification of the additional fourth level with the conduction band (thus indicating a charge-state conversion process) or its attribution to resonant energy transfer with surrounding lattice defects will require systematic dedicated studies.

The saturation emission intensity (Figure 5d) displayed a value of  $I_{\text{sat}} = (450 \pm 70)$  kcps, suggesting that the center is twice as bright as the SnV ZPL. Conversely, the optical power required to achieve the saturation ( $P_{\text{sat}} = (1.0 \pm 0.3)$  mW) is twice as higher.

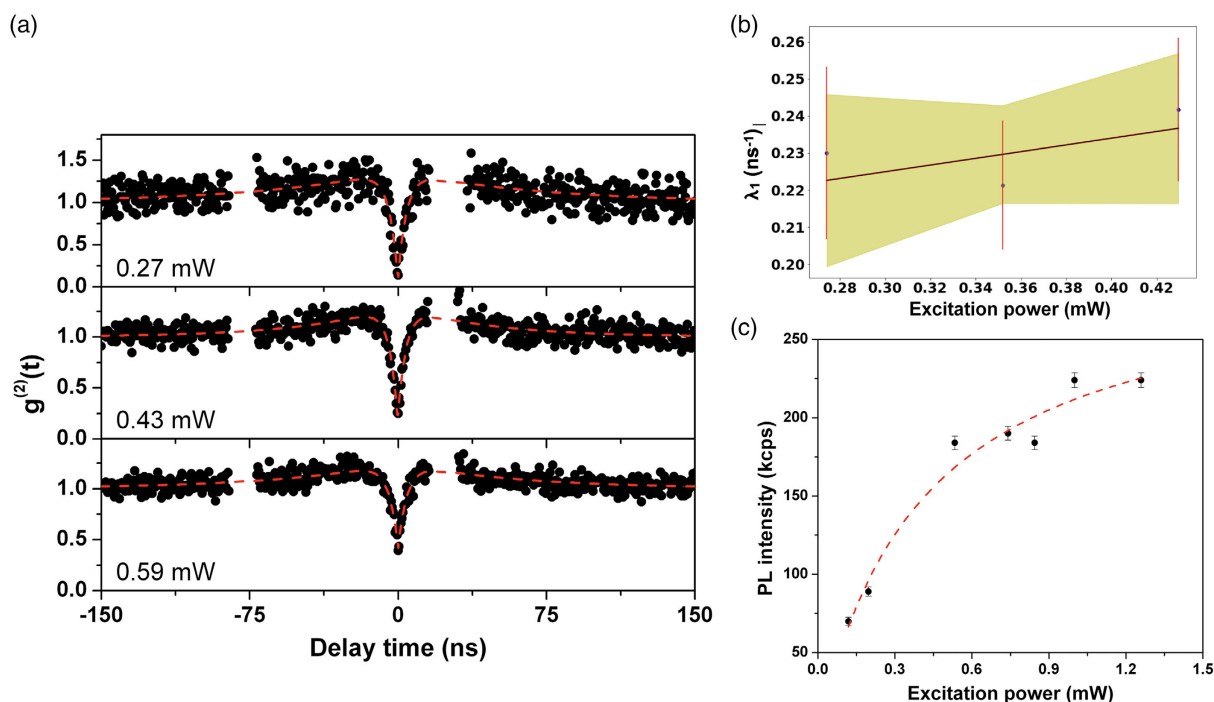


**Figure 5.** Characterization of the single-photon emission properties of an individual Sn-related defect emitting at the S2 line (631 nm, corresponding to the PL spectrum ii in Figure 1b). a) Second-order auto-correlation functions ( $g^{(2)}(t)$  curves shown without background-correction) acquired under 0.27, 0.43, and 0.59 mW laser excitation power. b) Linear fit of the decay constant  $\lambda_1$  extracted from the function fit of the  $g^{(2)}(t)$  curves as a function of the excitation power. c) Background-subtracted emission rate as a function of the laser excitation power. The red dashed line represents the fitting curve.

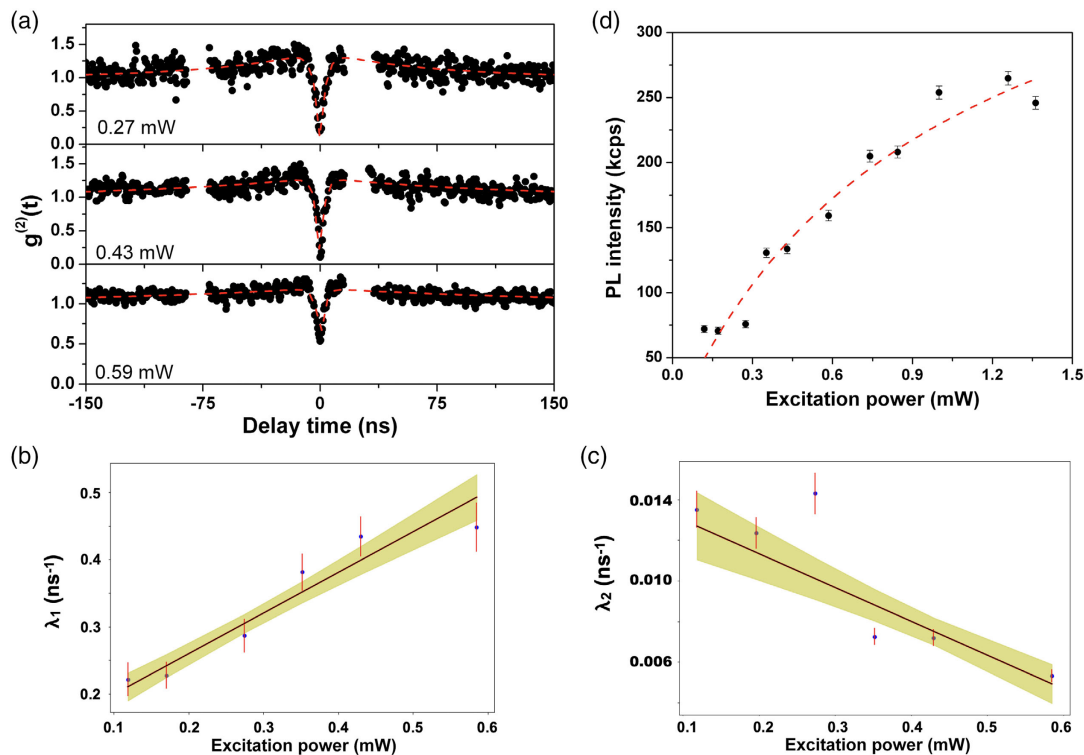


**Figure 6.** Characterization of the single-photon emission properties of an individual Sn-related defect emitting at the S3 line (647 nm), corresponding to the PL spectrum iii in Figure 1b. a) Second-order auto-correlation functions ( $g^{(2)}(t)$  curves shown without background-correction) acquired under 0.27, 0.43, and 0.59 mW laser excitation power. b) Linear fit of the decay constant  $\lambda_1$  extracted from the function fit of the  $g^{(2)}(t)$  curves as a function of the excitation power. c) Linear fit of the deshelling state lifetime parameter as a function of the laser excitation power. d) Background-subtracted emission rate as a function of the laser excitation power. The red dashed line represents the fitting curve.

**Table 1.** Summary of the emission properties of individual defects in Sn-implanted diamond.

Wavelength [nm]	Emission saturation intensity [kcps]	Emission saturation power [mW]	Excited state lifetime [ns]	Deshelling transition lifetime [ns]
620	$186 \pm 15$	$0.32 \pm 0.07$	$6.0 \pm 0.8$	$220 \pm 60$
631	$300 \pm 40$	$0.42 \pm 0.08$	$4.8 \pm 1.7$	NA
647	$450 \pm 70$	$1.0 \pm 0.3$	$7.4 \pm 1.0$	$68 \pm 9$

A summary of the relevant characterization parameters is reported in Table 1 for ease of comparison.

### 3. Conclusions

In this work, we reported the observation of multiple spectral emission lines at 620 nm (S1), 631 nm (S2), and 647 nm (S3) from individual defects formed upon Sn ion implantation in diamond and subsequent annealing, all of which were consistently observed in multiple previous reports.<sup>[6–8,12,14]</sup> The data presented here show for the first time the concurrent observation of all these three spectral contributions from the very same, single-photon emitting defect, suggesting among the possible

explanations their attribution to the same defect complex, that is, the SnV center.

We also investigated the occurrence of the S1–S3 lines as a function of the sample processing. The as-annealed substrate exhibited a prevalence of the S3 spectral feature among the spectral emission of  $\approx 40$  individual centers. Conversely, the S3 population density decreased in favor of the S1 emission line upon O-termination of the sample surface. This observation, in combination with the observation of both lines from the very same defect and of different emission lifetimes and intensity excitation saturation parameters, might suggest the attribution of the 647 nm PL peak to a different charge state of the defect, possibly neutral charge state of the SnV complex ( $\text{SnV}^0$ ), which has not been observed so far in other promising group-IV-related centers such as the GeV and the PbV.<sup>[4]</sup> This interpretation seems however to be ruled out by the findings recently reported in ref. [14], where the dynamical tuning of the diamond Fermi level by means of a p-i-p junction enabled to modulate the occurrence of the S1 emission line, but not that of the S3 spectral feature.

Conversely, the observation of a decreasing deshelling lifetime parameter  $\tau_2$  as a function of the laser excitation power suggests that the S3 emission might be related to a four-level system, a hypothesis that would not be in contrast with an energy transfer process involving the SnV center and surrounding radiation-induced defects generated upon ion implantation. This attribution will require a confirmation on centers fabricated upon



chemical vapor deposition synthesis or ion implantation followed by HPHT annealing, to rule out the role of local strains in the emergence of the 647 nm line. Conversely, its investigation as a function of the laser excitation wavelength will provide additional insight on charge state conversion mechanisms involved in the aforementioned emission. If confirmed, in analogy with what reported for the SiV<sup>0</sup> center,<sup>[39]</sup> a neutrally charged SnV complex might display strong insensitivity to environmental noise and therefore offer further increased spin coherence times and higher brightness, thus proving to be a natural candidate for the implementation of long-lived quantum memories.

## 4. Experimental Section

The measurements were performed on a high-purity single-crystal IIa diamond substrate with <100> orientation, denoted as “electronic grade” due to the <5 ppb concentration of both substitutional B and N impurities. A 200 × 200 μm<sup>2</sup> region was implanted using a collimated 60 keV Sn<sup>+</sup> ions at 2 × 10<sup>10</sup> cm<sup>-2</sup> fluence. The implantation was performed through a collimating steel mask placed at a ≈5 mm distance from the sample surface. This configuration allowed the implantation of stray ions at a lower fluence at the outer edge of the implanted region. This outer region was selected to observe and investigate Sn-related emitters at the individual level. The ions penetration range—estimated as 23 nm according to SRIM (stopping range of ions in matter) simulations<sup>[17]</sup>—was sufficiently close to the sample surface to consider the chemical terminations to be effective at tuning possible charge states of the lattice defects.<sup>[18]</sup>

The sample was subsequently annealed for 2 h in vacuum at 1200 °C to promote the formation of optically active defects. After the annealing process, residual surface conductivity was removed by an oxygen plasma treatment.

The PL characterization of individual defects was then performed under two different functionalization conditions of the sample surface: “as annealed,” that is, without any functionalization following a subsequent thermal annealing process (2 h, 950 °C), and after a plasma treatment in O<sub>2</sub> (experimental parameters: 60 Pa pressure, 0.5 sccm O<sub>2</sub> flux, 30 min duration, 23 W microwave power).

As mentioned earlier, the sample surface has a (100) orientation. It is broadly recognized that its chemical termination has a major effect on the local surface charge density of diamond, which in turn results in substantial variations on the charge state of color centers, as extensively investigated for the nitrogen-vacancy complex.<sup>[19]</sup> As widely ascertained in previous works, the as-CVD-grown (i.e., as-implanted) surface of the diamond sample is characterized by a hydrogen termination and is characterized by a negative electron affinity of 1.7 eV.<sup>[20]</sup> Thermal annealing in vacuum at temperatures exceeding 1000 °C results in the desorption of hydrogen from the sample surface<sup>[21]</sup> and in the rearrangement of carbon atoms at the surface involving the formation sp<sup>2</sup> bonds.<sup>[22]</sup> After this annealing process, once the sample surface is exposed to the environmental atmosphere, water contamination typically results in electron affinity values which are still negative.<sup>[23]</sup> Conversely, the exposure to oxygen plasma results in the oxygen termination of the surface, which is then characterized by a positive electron affinity of 2.4 eV.<sup>[24–26]</sup>

The PL emission of individual SnV centers was characterized by means of a fiber-coupled single-photon sensitive room-temperature confocal microscope already presented in previous works.<sup>[27]</sup> The confocal microscope was operated using a 520 nm CW laser excitation. A 600 nm long-pass filter enabled the minimization of the background associated with the Raman scattering (567 nm); at the same time, it prevented the investigation of the 593 nm emission line reported in previous works.<sup>[6,7,13,14]</sup> The spectral features of the emitters were analyzed using a single-grating monochromator (1200 grooves mm<sup>-1</sup>, 600 nm blaze, and ≈4 nm spectral resolution) fiber-coupled to a single-photon avalanche detector.<sup>[28]</sup>

## Acknowledgements

This work was supported by the following projects: Coordinated Research Project “F11020” of the International Atomic Energy Agency (IAEA); “Piemonte Quantum Enabling Technologies” (PiQuET) project funded by the Piemonte Region within the “Infra-P” scheme (POR-FESR 2014-2020 program of the European Union); “Departments of Excellence” (L. 232/2016), funded by the Italian Ministry of Education, University and Research (MIUR); “Ex post funding of research” project of the University of Torino funded by the “Compagnia di San Paolo”; “Intelligent fabrication of QUANTum devices in DIAMond by Laser and Ion Irradiation” (QuantDia) project funded by the Italian Ministry for Instruction, University and Research within the “FISR 2019” program; “Training on LASer fabrication and ION implantation of DEFects as quantum emitters” (LaslonDef) project funded by the European Research Council under the “Marie Skłodowska-Curie Innovative Training Networks” program; CSN5 “PICS4ME” experiment funded by the Italian National Institute of Nuclear Physics (INFN). The following projects leading to this publication have received funding from the EMPIR programme co-financed by the Participating States and from the European Union’s Horizon 2020 research and innovation programmes “Single-photon sources as new quantum standards” project: 17FUN06 SIQUST; “Beyond classical optical metrology” project: 17FUN01 (BeCOME); “Single- and entangled-photon sources for quantum metrology” project 20FUN05 (SEQUIME); “Quantum sensors for metrology based on single-atom-like device technology” project 20IND05 (QADeT). TL, SP and JM acknowledge the funding from the European Union’s Horizon 2020 research and innovation programme under grant agreement No 820394 (ASTERIQS).

## Conflict of Interest

The authors declare no conflict of interest.

## Data Availability Statement

The data that support the findings of this study are available from the corresponding author upon reasonable request.

## Keywords

annealing, charge, diamond, ion implantation, quantum, single-photon source, tin

Received: May 27, 2021

Revised: September 14, 2021

Published online: November 5, 2021

- [1] S. Prawer, *Quantum Information Processing with Diamond: Principles and Applications*, Woodhead Publishing, Cambridge 2014.
- [2] I. Aharonovich, D. Englund, M. Toth, *Nat. Photonics* **2016**, 10, 631.
- [3] T. Schröder, S. L. Mouradian, J. Zheng, M. E. Trusheim, M. Walsh, E. H. Chen, L. Li, I. Bayn, D. Englund, *J. Opt. Soc. Am. B* **2016**, 33, B65.
- [4] C. Bradac, W. Gao, J. Forneris, E. Trusheim, I. Aharonovich, *Nat. Commun.* **2019**, 10, 5625.
- [5] G. Pettrini, E. Moreva, E. Bernardi, P. Traina, G. Tomagra, V. Carabelli, I. P. Degiovanni, M. Genovese, *Adv. Quantum Tech.* **2020**, 2, 2000066.
- [6] T. Iwasaki, Y. Miyamoto, T. Taniguchi, P. Siyushev, M. H. Metsch, F. Jelezko, M. Hatano, *Phys. Rev. Lett.* **2017**, 119, 253601.
- [7] S. Ditalia Tchernij, T. Herzig, J. Forneris, J. Küpper, S. Pezzagna, P. Traina, E. Moreva, I. P. Degiovanni, G. Brida, N. Skukan,

- M. Genovese, M. Jaksic, J. Meijer, P. Olivero, *ACS Photonics* **2017**, *4*, 2580.
- [8] M. Alkahtani, I. Cojocar, X. Liu, T. Herzig, J. Meijer, J. Küpper, T. Lühmann, A. V. Akimov, P. Hemmer, *Appl. Phys. Lett.* **2018**, *112*, 241902.
- [9] A. E. Rugar, C. Dory, S. Sun, J. Vučković, *Phys. Rev. B* **2019**, *99*, 205417.
- [10] M. E. Trusheim, B. Pingault, N. H. Wan, M. Gündogan, L. De Santis, R. Debroux, D. Gangloff, C. Purser, K. C. Chen, M. Walsh, J. J. Rose, J. N. Becker, B. Lienhard, E. Bersin, I. Paradeisanos, G. Wang, D. Lyzwa, A. R.-P. Montblanch, G. Malladi, H. Bakhru, A. C. Ferrari, I. A. Walmsley, M. Atatüre, D. Englund, *Phys. Rev. Lett.* **2020**, *124*, 023602.
- [11] G. Thiering, A. Gali, *Phys. Rev. X* **2018**, *8*, 021063.
- [12] E. A. Ekimov, S. G. Lyapin, M. V. Kondrin, *Diam. Relat. Mater.* **2018**, *87*, 223.
- [13] T. Lühmann, R. John, R. Wunderlich, J. Meijer, S. Pezzagna, *Nat. Commun.* **2019**, *10*, 4956.
- [14] T. Lühmann, J. Küpper, S. Dietel, R. Staacke, J. Meijer, S. Pezzagna, *ACS Photonics* **2020**, *7*, 3376.
- [15] A. E. Rugar, H. Lu, C. Dory, S. Sun, P. J. McQuade, Z.-X. Shen, N. A. Melosh, J. Vuckovic, *Nano Lett.* **2020**, *20*, 1614.
- [16] G. Thiering, A. Gali, A., *NPJ Computational Materials* **2019**, *5*, 18.
- [17] J. F. Ziegler, M. D. Ziegler, J. P. Biersack, *Nucl. Instr. Meth. B* **2010**, *268*, 1818.
- [18] H. Yamano, S. Kawai, K. Kato, T. Kageura, M. Inaba, T. Okada, I. Higashimata, M. Haruyama, T. Tani, K. Yamada, S. Onoda, W. Kada, O. Hanaizumi, T. Teraji, J. Isoya, H. Kwarada, *Jap. J. Appl. Phys.* **2017**, *56*, 04CK08.
- [19] H. Pinto, R. Jones, D. W. Palmer, J. P. Goss, A. K. Tiwari, P. R. Briddon, N. G. Wright, A. B. Horsfall, M. J. Rayson, S. Öberg, *Phys. Rev. B* **2012**, *86*, 045313.
- [20] S. J. Sque, R. Jones, P. R. Briddon, *Phys. Rev. B* **2006**, *73*, 085313.
- [21] C. Su, J.-C. Lin, *Surf. Sci.* **1998**, *406*, 149.
- [22] V. L. Kuznetsov, I. L. Zilberberg, Y. V. Butenko, A. L. Chuvilin, *J. Appl. Phys.* **1999**, *86*, 863.
- [23] X. Gao, L. Liu, D. Qi, S. Chen, A. T. S. Wee, T. Ouyang, K. P. Loh, X. Yu, H. O. Moser, *J. Phys. Chem. C* **2008**, *112*, 2487.
- [24] M. M. Hassan, K. Larsson, *J. Phys. Chem. C* **2014**, *118*, 22995.
- [25] J.-P. Chou, A. Gali, *MRS Commun.* **2017**, *7*, 551.
- [26] V. Petraková, A. Taylor, I. Kratochvilova, F. Fendrych, J. Vacik, J. Kucka, J. Stursa, P. Cicler, M. Ledvina, A. Fiserova, P. Kneppo, M. Nesladek, *Adv. Funct. Mater.* **2012**, *22*, 812.
- [27] G. Prestopino, M. Marinelli, E. Milani, C. Verona, G. Verona-Rinati, P. Traina, E. Moreva, I. P. Degiovanni, M. Genovese, S. Ditalia Tchernij, F. Piccolo, P. Olivero, J. Forneris, *Appl. Phys. Lett.* **2017**, *111*, 111105.
- [28] S. Ditalia Tchernij, E. Corte, T. Lühmann, P. Traina, S. Pezzagna, I. P. Degiovanni, G. Provatas, E. Moreva, J. Meijer, P. Olivero, M. Genovese, J. Forneris, *New J. Phys.* **2021**, *23*, 063032.
- [29] J. M. Binder, A. Stark, N. Tomek, J. Scheuer, F. Frank, K. D. Jahnke, C. Müller, S. Schmitt, M. H. Metsch, T. Unden, T. Gehring, A. Huch, U. L. Andersen, L. J. Rogers, F. Jelezko, *Software X* **2017**, *6*, 85.
- [30] A. Beveratos, R. Brouri, T. Gacoin, J.-P. Poizat, P. Grangier, *Phys. Rev. A* **2001**, *64*, 061802.
- [31] M. V. Hauf, B. Grotz, B. Naydenov, M. Dankerl, S. Pezzagna, J. Meijer, F. Jelezko, J. Wrachtrup, M. Stutzmann, F. Reinhard, J. A. Garrido, *Phys. Rev. B* **2011**, *83*, 081394.
- [32] D. Gatto Monticone, P. Traina, E. Moreva, J. Forneris, P. Olivero, I. P. Degiovanni, F. Taccetti, L. Giuntini, G. Brida, G. Amato, M. Genovese, *New J. Phys.* **2014**, *16*, 053005.
- [33] Z. Mu, Y. Zhou, D. Chen, J. E. Fröch, J. Tang, X. Li, I. Aharonovich, W.-B. Gao, *Adv. Opt. Mater.* **2020**, *8*, 2000495.
- [34] S. C. Kitson, P. Jonsson, J. G. Rarity, P. R. Tapster, *Phys. Rev. A* **1998**, *58*, 620.
- [35] T. Iwasaki, F. Ishibashi, Y. Miyamoto, Y. Doi, S. Kobayashi, T. Miyazaki, K. Tahara, K. D. Jahnke, L. J. Rogers, B. Naydenov, F. Jelezko, S. Yamasaki, S. Nagamachi, T. Inubushi, N. Mizuochi, M. Hatano, *Sci. Rep.* **2015**, *5*, 12882.
- [36] J. Görlitz, D. Herrman, G. Thiering, P. Fuchs, M. Gandil, T. Iwasaki, T. Taniguchi, M. Kieschnick, J. Meijer, M. Hatano, *New J. Phys.* **2020**, *22*, 13048.
- [37] E. Neu, M. Agio, C. Becher, *Opt. Express* **2012**, *20*, 19956.
- [38] M. Nagra, D. Alshamaa, R. Deturche, V. Davydov, L. Kulikova, V. Agafonov, C. Couteau, *AVS Quant. Sci.* **2021**, *3*, 012001.
- [39] B. C. Rose, D. Huang, Z.-H. Zhang, P. Stevenson, A. M. Tryshkin, S. Sangtawesin, S. Srinivasan, L. Loudin, M. Markham, A. M. Edmonds, D. J. Twitchen, S. A. Lyon, N. P. de Leon, *Science* **2018**, *63*, 60.
- [40] A. Meda, I. P. Degiovanni, A. Tosi, Z. Yuan, G. Brida, M. Genovese, *Light* **2017**, *6*, 1626.